Design of three-dimensional engineered protein hydrogels for tailored control of neurite growth

Kyle J. Lampe, Alexander L. Antaris, Sarah C. Heilshorn *

Materials Science and Engineering Department, Stanford University, Stanford, CA 94305, USA

ABSTRACT

The design of bioactive materials allows tailored studies probing cell–biomaterial interactions, however, relatively few studies have examined the effects of ligand density and material stiffness on neurite growth in three-dimensions. Elastin-like proteins (ELPs) have been designed with modular bioactive and structural regions to enable the systematic characterization of design parameters within three-dimensional (3-D) materials. To promote neurite out-growth and better understand the effects of common biomaterial design parameters on neuronal cultures we here focused on the cell-adhesive ligand density and hydrogel stiffness as design variables for ELP hydrogels. With the inherent design freedom of engineered proteins these 3-D ELP hydrogels enabled decoupled investigations into the effects of biomechanics and biochemistry on neurite out-growth from dorsal root ganglia. Increasing the cell-adhesive RGD ligand density from 0 to 1.9×10^7 ligands μm^{-3} led to a significant increase in the rate, length, and density of neurite out-growth, as quantified by a high throughput algorithm developed for dense neurite analysis. An approximately two-fold improvement in total neurite out-growth was observed in materials with the higher ligand density at all time points up to 7 days. ELP hydrogels with initial elastic moduli of 0.5, 1.5, or 2.1 kPa and identical RGD ligand densities revealed that the most compliant materials led to the greatest out-growth, with some neurites extending over 1800 μm by day 7. Given the ability of ELP hydrogels to efficiently promote neurite out-growth within defined and tunable 3-D microenvironments these materials may be useful in developing therapeutic nerve guides and the further study of basic neuron–biomaterial interactions.

© 2012 Acta Materialia Inc. Published by Elsevier Ltd. All rights reserved.

1. Introduction

Injuries to and diseases of the peripheral and central nervous systems lead to dysfunction and loss of neuronal tissue. The neurons responsible for signal transmission have limited regenerative potential to bridge large tissue defects and are rarely able to re-establish distant axonal connections [1,2]. Extension of long neurites, the collective term for neuronal processes of axons and dendrites, remains a challenge for both endogenous and transplanted neurons [3]. A multitude of biomaterials have been developed to promote neurite growth, including high water content hydrogels formed from both natural and synthetic sources [4]. Natural hydrogels such as collagen and fibrin gels successfully promote extensive neurite out-growth [5–8], but their material properties can vary depending on source location and species [9,10]. This prevents systematic control of the biochemical and biomechanical design parameters known to have an impact on neurite extension. In contrast, engineered material systems enable this design control,

allowing investigators to dictate molecular structure, functional bioactivity, and resulting cell–material interactions [11–15].

Elastin-like proteins (ELPs) are produced by recombinant protein synthesis yielding engineered protein polymers made entirely of amino acids. This synthetic strategy dictates exact materials design from the molecule up, providing an orthogonal approach to traditional synthetic polymerization techniques for creating tunable bioactive matrices that can control cell function [16]. The high fidelity transcription and translation processes are a precise and accurate synthesis method resulting in biopolymers with exact specificity of the amino acid monomer sequence and no polydispersity. These proteins are designed by mimicking the useful functionalities found in native matrix proteins. The modular combination of multiple functional peptide sequences enables the rational design of entirely new proteins with specified biomaterial design parameters. In ELPs, repetitive short elastin-like structural sequences (Fig. 1) confer material elasticity and resilience without any known cell interaction domains [17]. Selected bioactive sequences can be interspersed between these elastin-like domains to enable specific cell adhesion interactions [18] and tailored rates of enzymatic degradation [19]. To date these ELPs have been used in cell culture for only two-dimensional (2-D) studies identifying

* Corresponding author. Tel.: +1 650 723 3763; fax: +1 650 498 5596.
E-mail address: heilshorn@stanford.edu (S.C. Heilshorn).
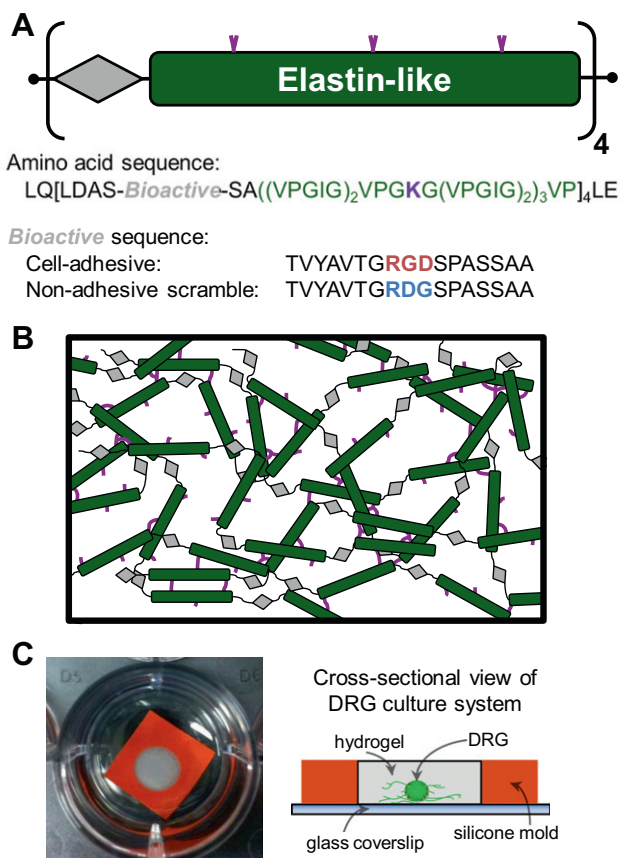
Fig. 1. Schematic of ELP design and hydrogel network. (A) ELPs were designed with modular repeats of bioactive (grey diamond) and elastin-like (green bar) sequences. The bioactive domains were either an extended RGD sequence to confer the engineered protein with cell adhesion ligands or a non-adhesive scrambled RDG sequence. (B) The elastin-like structural domains included lysines (purple) for site-specific crosslinking with primary amine-reactive crosslinkers yielding a 3-D hydrogel network. (C) Photograph (left) and schematic (right) of ELP crosslinked into an amorphous, semi-translucent hydrogel using a 5 mm silicone mold (orange) to encapsulate a single DRG cluster and culture the system within a 24-well plate.

therefore, tunable materials that allow for cell–material interactions in all three dimensions.

Biomechanics and cell-adhesive ligand density are two critical regulators of neurite out-growth that can be tuned to create extracellular matrix (ECM)-like microenvironments. First, the stiffness of a supporting matrix is known to be a major factor determining the behavior of cultured neural cells [22–25,31]. Brain and spinal cord matter are some of the most compliant human tissues, and as such it has been hypothesized that compliant hydrogels are most well suited to induce neural regeneration [2]. In many cases significant improvements in neurite growth [22,24,25,31] and neuronal differentiation from neural stem cells (NSCs) [23,32] were reported for biomaterials with the lowest stiffness tested. Others have shown enhanced NSC proliferation and differentiation at intermediate stiffnesses that closely match the mechanical properties of native neural tissue [22,23]. In addition to stiffness, independent control of cell-adhesive ligand density is a well-known important design parameter controlling cell function [13,24,33]. The RGD ligand has been specifically incorporated into a number of biomaterials and tuned to examine location- and concentration-dependent effects on neurite length and branching [20,24,34–36]. Cells may respond to these biomechanical and biochemical cues in a context-dependent manner [24], thus having independent control of each parameter within the same biomaterial can enable systematic evaluation of cell–material interactions.

Here our goal was to design a family of ELP hydrogels to promote out-growth of neurites in a 3-D environment and to better understand the effects of biomaterial design parameters on the rate, length, and density of neurite growth. These amorphous 3-D matrices allowed viable encapsulation and extensive neurite growth from explanted chick dorsal root ganglia (DRG), a commonly studied tissue composed of neurons and glia found at the interface between the central and peripheral nervous systems. Individual neurites were surrounded by matrix and grew in multiple focal planes, thus demonstrating the three-dimensionality of the system. Through the use of an in-house-designed, automated image processing algorithm we show that the biomechanical and cell-adhesive biochemical parameters of ELP hydrogels both have profound effects on the neurite length distribution, longest neurite out-growth distance, and total out-growth. Tuning the cell-adhesive RGD density from 0 to 1.9×10^7 ligands μm^{-3} while maintaining a constant modulus of 1.5 kPa resulted in a roughly two-fold increase in total DRG neurite out-growth over 7 days in 3-D culture. In contrast, the tuning of initial elastic modulus from 0.5 to 2.1 kPa by adjusting the matrix crosslink density while maintaining a constant 1.9×10^7 RGD ligands μm^{-3} inhibited neurite out-growth across all time points tested. These results demonstrate the usefulness of ELP hydrogels to present systematically controlled and defined 3-D microenvironments to neuronal cultures, thereby allowing multi-functional and independent control over the cell-adhesive and biomechanical properties that influence cell behavior.

2. Materials and methods

2.1. Elastin-like polypeptide synthesis and purification

ELPs were designed and synthesized as previously reported with a cell-adhesive, fibronectin-derived extended RGD sequence or a non-adhesive RDG scrambled sequence (Fig. 1) [20]. Briefly, the encoding plasmid was transformed into the BL21 (DE3) strain of *Escherichia coli*. Cultures were grown to an OD_{600} of 0.8. Protein production was induced under the T7-lac promoter with 1 mM isopropyl β-D-1-thiogalactopyranoside (IPTG) for 4–6 h. Cell pellets were harvested and lysed by sonication in TEN buffer (0.1 M NaCl,

the effect of cell-adhesive ligand density on neurite out-growth of PC12 cells, a model neuron-like cell line [20].

While traditional cell culture utilizes stiff, planar, 2-D substrates, recent results have highlighted the importance of dimensionality for neuronal culture, with three-dimensional (3-D) matrices critically affecting neural metabolic activity, growth, and phenotype [21,22]. Much has been learned regarding neural cell–cell and cell–material interactions by studying cells seeded on biomaterials in two dimensions [8,23–25] and in some cases allowing for migration into the material (termed 2.5-D) [26]. However, in two dimensions cells must reorganize their integrin cell surface receptors and cytoskeleton to adapt to the planar presentation of receptor ligands, leading to distinct dynamic and spatial differences in the distribution of cell–cell and cell–matrix interactions compared with three dimensions [27–29]. In a 3-D environment cells are no longer restricted to a polarized, planar geometry, as they sense and respond to stimuli from multiple directions with differentially distributed traction forces [30]. In the case of neurons dimensionality plays a major role in neurite extension, retraction, branching, and maturation into axons and dendrites. As a result, neurons cultured in 3-D versus 2-D environments display strikingly distinct morphologies, with 3-D cultures resulting in neuritic geometries more representative of those which occur in vivo [21]. These data strongly suggest that the development of biomaterials for neural regenerative applications requires 3-D analysis and,

0.01 M Tris, 0.001 M EDTA salt, pH 8) with 1 mM phenylmethylsulfonyl fluoride protease inhibitor. ELP was purified by iterative temperature cycling and centrifugation at 4 °C in H_2O (pH 9) to collect ELP in solution, followed by 37 °C in 1 M NaCl to pellet the ELP. Purity was confirmed by SDS–PAGE. Purified ELP was dialyzed against H_2O using a 10,000 molecular weight cut-off membrane and lyophilized.

2.2. Hydrogel crosslinking and DRG encapsulation

Lyophilized ELP was dissolved at 3.75 wt.% in phosphate-buffered saline (PBS) overnight at 4 °C with agitation. ELP solutions were then sterile filtered (0.22 μm pore size) and kept on ice. Tetrakis(hydroxymethyl)phosphonium chloride (THPC) crosslinker solution was diluted in PBS to the appropriate concentration, sterile filtered, and kept on ice.

DRG were isolated from embryonic day 9 (E9) chicks and collected in sterile medium containing 10% fetal bovine serum (FBS) and 1% penicillin/streptomycin. A similar hydrogel encapsulation protocol to that previously reported was used [37]. Individual DRGs were placed in 5 mm diameter molds of silicone rubber (height 0.5 mm) affixed to glass coverslips. ELP and THPC solutions were mixed at 80:20 vol.%, and 15.5 μl added to each DRG to fill the hydrogel mold, resulting in a final amorphous scaffold of 3.0 wt.% (Fig. 1C). In the case of RGD density experiments the ratio of crosslinker reactive groups (4 hydroxymethyl groups per THPC molecule) to ELP reactive sites (14 primary amines per molecule) was kept constant at 1:1 using a THPC crosslinker stock solution of 2.64 mg ml^{-1}. For hydrogels with different crosslink densities the concentration of THPC was adjusted to achieve reactive site ratios of 0.5:1, 1:1, and 2:1, using THPC solutions of 1.32, 2.64, and 5.28 mg ml^{-1}, respectively.

Hydrogels were allowed to polymerize at room temperature for 10 min, followed by 10 min at 37 °C, during which time the ELP hydrogels become opaque. The hydrogels were then flooded with warm DRG culture medium consisting of 10% FBS and 1% penicillin/streptomycin in Dulbecco's modified Eagle's medium (DMEM) supplemented with 50 ng ml^{-1} nerve growth factor (NGF) according to the literature [8,38–40]. DRGs were cultured at 37 °C in 5% CO_2 and 100% humidity. The medium was exchanged every 2 days.

2.3. Hydrogel mechanical properties determination

Hydrogels were crosslinked as above on top of glass microscope slides. The silicon mold was carefully removed and the hydrogel immersed in a pool of PBS at 37 °C. The elastic modulus in compression mode was determined by generating stress–strain curves in unconfined compression to 15% strain. Curves were normalized by subtracting the baseline force of wet runs in PBS alone. The mass swelling ratio was calculated from the hydrogel wet mass divided by the dry mass after lyophilization. All measurements were in triplicate.

2.4. Cell staining and confocal microscopy

DRGs encapsulated in 3-D ELP hydrogels ($n > 7$ for each hydrogel condition with at least 3 independent experiments) were briefly rinsed twice with PBS and stained with Live/Dead solution containing 2 μM calcein acetoxymethylester and 4 μM ethidium homodimer-1 in DMEM without phenol red for 45 min at 37 °C, 5% CO_2, and 100% humidity. After staining the gels were rinsed twice with PBS and immediately imaged as a 3-D stack using confocal microscopy (Leica SPE). z-stacks of greater than 100 μm depth into the hydrogel were created with 2.4 μm intervals between slices and compressed into a maximum projection image. The opacity of the ELP hydrogels prevented imaging deeper penetration

depths with this microscopy set-up. When images of a large field of view were required the Leica LAS AF software was used to automate xy tiling and facilitate image stitching. Percent cell viability was quantified by counting the number of green pixels and dividing by the total number of red and green pixels in maximum projection images.

For immunocytochemistry hydrogels were rinsed briefly with PBS and fixed overnight in 4% paraformaldehyde at 37 °C. The remaining procedures were carried out at room temperature. Samples were washed four times in PBS, permeabilized with 0.25% Triton X-100 in PBS for 30 min, washed twice with PBS, and blocked with 5% bovine serum albumin (BSA) and 0.5% Triton X-100 in PBS for 90 min. Samples were then incubated overnight with primary antibody (mouse anti-β-tubulin, 1:500, and rabbit anti-S100, 1:400, diluted in 2.5% BSA and 0.5% Triton X-100 in PBS) and rinsed three times in PBS for 60 min each. Finally, the samples were incubated with secondary antibodies (goat anti-mouse, 1:500, and goat anti-rabbit, 1:500) with Hoescht (1:5000) overnight and washed more than six times for 30 min each in PBS. Images were collected using a Leica SPE confocal microscope as described above.

2.5. Image processing and data analysis

A Matlab code was written to analyze maximum projection images of the live/dead stained DRGs, as the high neurite outgrowth density prevented processing with existing neurite tracking software such as NeuronJ. A threshold filter was applied to maximum projection images of live cells to obtain binary black/white images. The initial DRG explant boundary was manually outlined, and the Matlab code calculated the explant center of mass. Neurite extension lengths for a single explant were measured along 360 radial directions from the explant center of mass in 1° increments. For each radial vector the neurite "start point" was defined as the initial explant boundary and the neurite "end point" was defined as the last valued pixel. Neurite lengths were grouped into 50 μm bins to generate a histogram for each individual DRG culture. Histograms were grouped and averaged for each hydrogel condition, and statistical significance was evaluated using the Kolmogorov–Smirnov test. The longest neurite and total neurite outgrowth data are presented as means ± standard deviation. Statistical significance was determined using a single tailed t-test assuming unequal variances and $P < 0.05$.

2.6. Hydrogel molding into a two-layered, composite cylindrical conduit

An agarose cylinder (outer diameter ∼3 mm) was inserted within a ∼20 mm length of silicone tubing (inner diameter ∼5 mm), leaving a ring-shaped gap of ∼2 mm gap on all sides. This gap was filled with 10 wt.% ELP solution mixed with a 1:1 stoichiometric ratio of THPC crosslinker and ∼2 drops of blue food coloring to enhance visualization. After polymerization, as described above, the agarose cylinder core and silicone tubing were removed, leaving a cylindrical conduit of ELP. This conduit was filled with a second ELP solution of 3 wt.% ELP mixed with THPC crosslinker (1:1 stoichiometric ratio) and ∼2 drops of red food coloring to distinguish the solution from the outer conduit.

3. Results and discussion

3.1. Independent tuning of hydrogel RGD density and modulus

Hydrogel crosslink density was tuned by adjusting the THPC crosslinker concentration while maintaining a constant protein polymer concentration at 3.0 wt.%. As expected, increasing the stoichiometric ratio of total THPC reactive sites (4 per molecule)

to primary amines present in our ELP (14 per molecule) from 0.5:1 to 1:1 to 2:1 increased the initial elastic modulus of the resulting amorphous hydrogel (E = 0.5, 1.5, and 2.1 kPa, respectively, Fig. 2A). By designing exactly four cell-adhesive RGD ligands into each ELP molecule and by maintaining a constant protein concentration with the engineered matrices we were able to tune the hydrogel network crosslink density without varying the cell-adhesive ligand density. This provides a distinct advantage over performing such studies with native or harvested proteins such as collagen or fibrin. In such cases it is difficult to decouple cell-adhesive ligand density and stiffness, as changing the protein concentration to tune the modulus also leads to differences in the density of cell-adhesive ligands.

Alternatively, ELPs facilitated making crosslinked hydrogels of similar mechanical properties while tailoring the RGD cell-adhesive ligand density. The ability to control cell-binding ligand type and density, and thus to study their effects on cell morphology and differentiation, has proven to be a useful strategy for understanding specific cell–matrix interactions and utilizing them to induce a desired cell response [13,24,33]. The modular design of our engineered protein facilitates the creation of identical ELPs that differ only in the bioactive RGD ligand sequence. Using recombinant protein technology an otherwise identical ELP was synthesized that included a negative control, non-cell-adhesive, scrambled RDG sequence. Homogenous mixing of ELPs with and without the putative RGD cell-adhesive sequence enabled creation

of hydrogels with RGD densities of 0, 0.96×10^7, and 1.9×10^7-ligands cm^{-3} (0, 1.6, and 3.2 mM, respectively). As expected, because all ELP hydrogels had a total protein content of 3 wt.%, the resulting mass swelling ratios were found to be statistically identical (16.3, 15.8, and 16.3, respectively, Fig. 2B). These results validate the use of the lysine-reactive crosslinker THPC to enable independent tuning of crosslink density and cell-adhesive ligand density within 3-D ELP hydrogel microenvironments.

3.2. 3-D culture of DRGs in ELP hydrogels

To evaluate the cytocompatibility of this 3-D biomaterial we quantified the viability of embryonic chick DRGs encapsulated within the family of crosslinked ELP hydrogels. As demonstrated by live/dead staining with calcein AM and ethidium homodimer, respectively, DRG explants were highly viable after encapsulation, with only a small fraction of dead cells observed at early time points (Fig. 2C). Quantification of multiple crosslinking experiments ($n \geqslant 7$ for each hydrogel design) demonstrated that neither RGD density nor crosslink density had a significant impact on survival after encapsulation (Fig. 2D). In all cases viability of the stained cells was greater than 79% (Fig. 2D) and increased over time as the neurites grew and extended outward from the initial explant. The THPC crosslinking mechanism, which covalently reacts with primary amines, may react with cell surface proteins, potentially resulting in the isolated cell death observed at early time points. Alternatively, this initial cell death may be the result of DRG tissue isolation resulting in axon severing and loss of cell–cell contacts. While few studies have quantified neuronal viability in 3-D, our cell viability was consistent with that observed for dissociated DRG neurons encapsulated in Puramatrix peptide gels [41] and PEG–fibrinogen gels [42]. THPC therefore affords a readily available, cost-effective, and water soluble mechanism to produce cytocompatible crosslinked hydrogels.

In the work here the small amount of cell death observed did not appear to inhibit neural regeneration of encapsulated neurons, as they rapidly extended neurites into the surrounding 3-D matrix. In these engineered protein hydrogels neurites may be able to extend if the initial mesh size is sufficiently large to allow penetration or if cells proteolytically degrade the local matrix to increase the mesh size. In the absence of proteases ELP hydrogels are hydrolytically stable for at least 4 weeks, with no evidence of degradation [19]. Neurites quickly emerged from the explanted tissue and extended into the matrix in all directions as early as day 1 in most cases (Fig. 3A). This out-growth occurred in multiple planes to the maximum imaging depth of approximately 100 μm (Fig. 3A), indicating that neurite growth was not limited to the underlying coverslip. Previous studies of cells on compliant hydrogels with similar elastic moduli to the materials used here (~1–5 kPa) have demonstrated that cells may be capable of "sensing" an underlying rigid substrate such as a glass coverslip. For mesenchymal stem cells, which can exert matrix stresses of hundreds of piconewtons per square micrometer, the estimated depth to which the cells can sense the underlying stiff mechanical interface is 1–3.4 μm [43,44]. In contrast, neurons are capable of exerting much smaller stresses of the order of 30 pN μm^{-2} [45], therefore, they are even less sensitive to the underlying rigid substrate. A conservative estimate is that only those neurons within 1–2 μm of the interface may be affected by the rigid coverslip. In other words, we hypothesize that 98–99% of the total 100 μm imaging depth includes neurites that are fully surrounded by a 3-D hydrogel matrix without sensing the underlying stiff substrate. We further confirmed this hypothesis by evaluating neurite out-growth at various hydrogel depths, as discussed below in Section 3.5 and as shown in Supplementary Fig. S1. Neural culture within such a 3-D
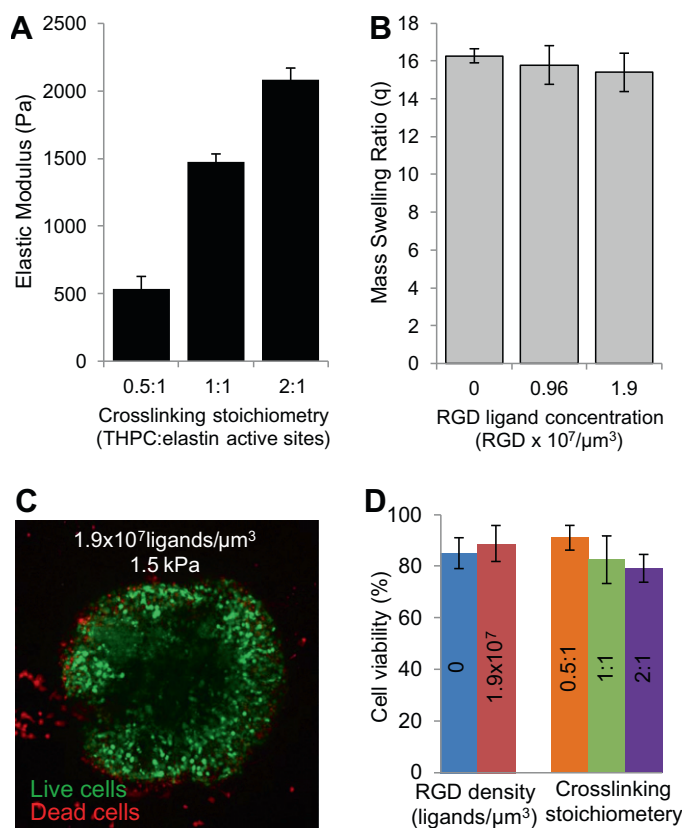
Fig. 2. Mechanical properties of ELP hydrogels and cell encapsulation viability. (A) Increasing the ratio of THPC reactive sites to primary amines in the ELP led to an increase in hydrogel elastic modulus without any changes in RGD adhesive ligand density. (B) Alternatively, the density of bioactive RGD ligands in a hydrogel was tuned without changing the hydrogel mechanical properties, as shown by the mass swelling ratio. (C) DRG explants after 1 day culture stained live (green) and dead (red) indicated only a small number of dead cells in the periphery of the DRG. (D) Viability on day 1 indicated that cell survival was not affected by variations in the hydrogel RGD ligand density or hydrogel crosslink density.
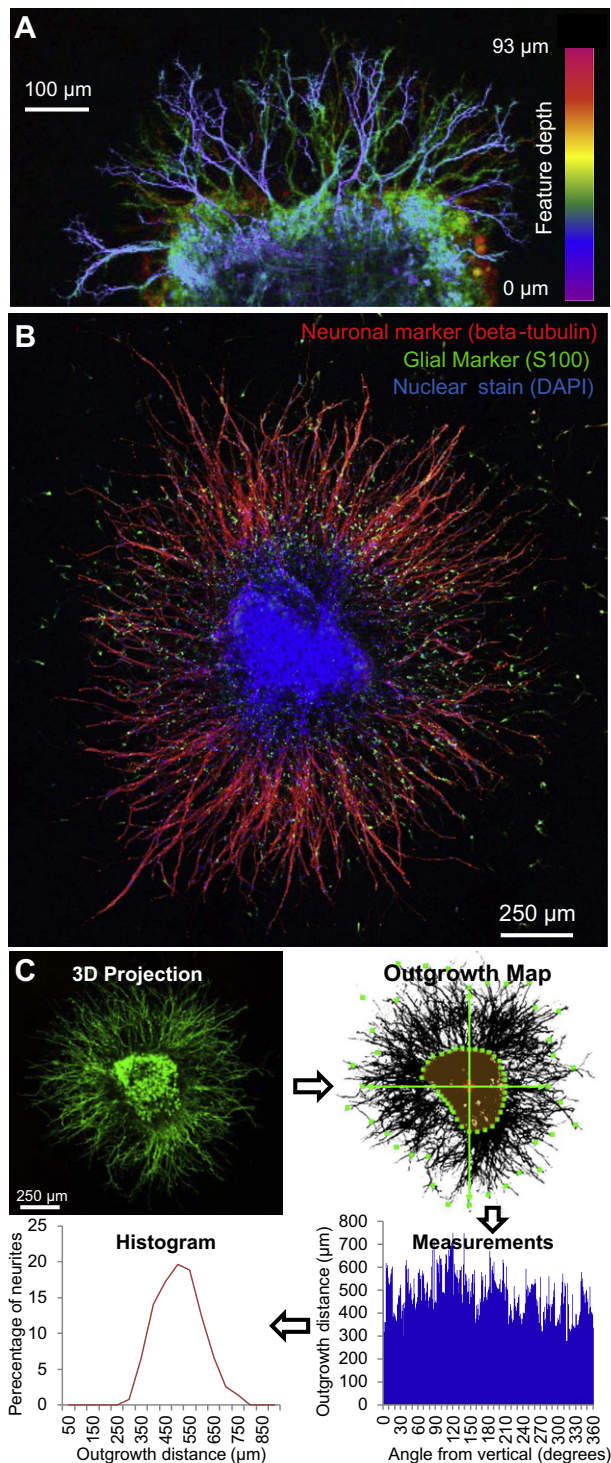
Fig. 3. Characterization and quantification of 3-D neurite growth from DRGs. (A) Neurites extended in multiple planes throughout the 3-D ELP matrix as visualized by a maximum projection image of live cell staining throughout a 93 μm z-stack. (B) The growth observed from DRG explants was primarily neurites extending from β-tubulin positive neurons (red). Few S100 positive glial cells (green) migrated into the matrix. (C) Clockwise from upper left, maximum projection images were created from 3-D z-stacks of live/dead stained DRGs. The initial explant area was manually traced (highlighted in orange) and an in-house algorithm was used for quantification of the dense neurite growth. The Euclidian distance from the initial DRG explant boundary to the most distant out-growth was determined at 1° increments radially from the initial DRG explant center of mass (center of mass marked with a cross, example start/end points of out-growth marked with green boxes). This yielded neurite out-growth distance measurements at each degree angle. For each DRG these were plotted as a histogram grouping neurite lengths into 50 μm bins.

environment removes the spatial constraints of traditional 2-D cultures for migration and neurite extension [27,46].

Immunostaining demonstrated that the out-growth was indeed neurite extension, as the majority of the growth was positive for the neuronal marker β-tubulin, with very few glial cells migrating into the matrix (Fig. 3B). For potential therapeutic applications modulating glial migration and proliferation may be important in enhancing injury repair. In the peripheral nervous system this may include stimulating Schwann cell activation to promote axon regeneration [47], whereas in the central nervous system it is desirable to prevent the glial over-growth commonly observed after injury, where formation of a glial scar inhibits axon and dendrite regeneration [48]. This scar-like behavior has also been reported to occur when mixed populations of neural cells are cultured on stiff 2-D tissue culture polystyrene plates and other stiff material systems [22].

3.3. High throughput quantification of neurite out-growth

Accurately quantifying neurite growth is a technically challenging but key focus for studies of neuronal regeneration. Even simplified measures of neurite extension, such as the "longest" neurite length measurement often employed, can require laborious image analysis. Over the last decade significant progress has been made in developing computational tools to analyze images of neurons and neuronal networks. The large selection of software now available to quantify neurite growth generally involves the identification of the cell body followed by either "global" techniques, i.e. whole image processing involving thresholding and skeletalization of the neuronal tree (axons and dendrites), or by "local" techniques, i.e. systematic exploration that iteratively predicts points along a neurite, effectively tracing out axons and dendrites [49]. Unfortunately, much of this software, including NeuronJ and Neurolucida, is designed to process images containing sparse populations of neurons and is not suited for the analysis of the very dense growth resulting from DRGs encapsulated in our hydrogels. Furthermore, culturing cells in a 3-D environment further complicates the ability to generate accurate and representative data. Consequently, we developed a high throughput method to quantify large numbers of neurites from many independent samples.

Each sample was imaged in 3-D to greater than 100 μm depth using a 2.4 μm step size, and the resulting image stack was compressed into a maximum projection image (Fig. 3C, upper left). Pre-processing steps including thresholding and transformation into a binary representation were applied uniformly across all images. After manually tracing the initial DRG explant boundary the search algorithm automatically quantified neurite out-growth around the DRG by measuring the Euclidean distance between the initial explant boundary and the furthest neurite growth (Fig. 3C, upper right). By repeating this measurement at 1° intervals around the entire explant center of mass a detailed dataset was collected that included information about the neurite out-growth distance, neurite out-growth density, and distribution of neurite out-growth from each DRG (Fig. 3C, bottom right). These data can be displayed as a histogram of neurite out-growth distance, which shows the distribution of neurite out-growth for an individual sample (Fig. 3C, bottom left). The algorithm facilitates rapid analysis of a large number of samples, therefore, several histograms were obtained for multiple independent samples for each biomaterial condition and time point ($n > 7$ per condition). Furthermore, the algorithm enables further data analysis to report common measurements of neurite extension, such as longest neurite out-growth distance and total neurite out-growth (Figs. 4 and 5) [6]. Using this method we quantified 148 DRG samples, resulting in more than 53,000 individual distance measurements, to present

an accurate distribution of neurite out-growth, both within a single DRG sample and between samples.

3.4. Cell-adhesive RGD ligands enhance neurite out-growth

Two otherwise identical protein-based ELP biomaterials were fabricated, one with a cell-adhesive, fibronectin-derived RGD sequence and another containing a scrambled sequence, non-adhesive RDG peptide. DRGs were encapsulated within these two biomaterials, estimated to contain ligand densities of 0 and 1.9×10^7 ligands μm^{-3}, respectively ($n = 8$–16 per condition and time point from at least 4 different experiments). This enabled direct comparison of matrices with distinctly different cell-adhesive characteristics yet identical mechanical properties (reactive site ra-

tio of 1:1, initial modulus = 1.5 kPa) (Fig. 2B). RGD density had a profound effect on both the out-growth distance and density of neurites (Fig. 4A). Consistent with previous reports, cells exhibited some minimal growth and neurite extension in the absence of RGD ligands, presumably due to synthesis of their own ECM [14,22].

After 1 day culture over 50% of neurite out-growth had Euclidean distances of less than 50 μm for both the 0 and 1.9×10^7 ligands μm^{-3} samples. Statistical analysis by Kolmogorov–Smirnov testing showed that the population distributions were already statistically different on day 1 and became increasingly distinct throughout the 7 day culture period (Fig. 4B), indicating that the rate of neurite growth was enhanced in the presence of the RGD ligand. There were significant heterogeneities observed between different DRG samples within the same experimental
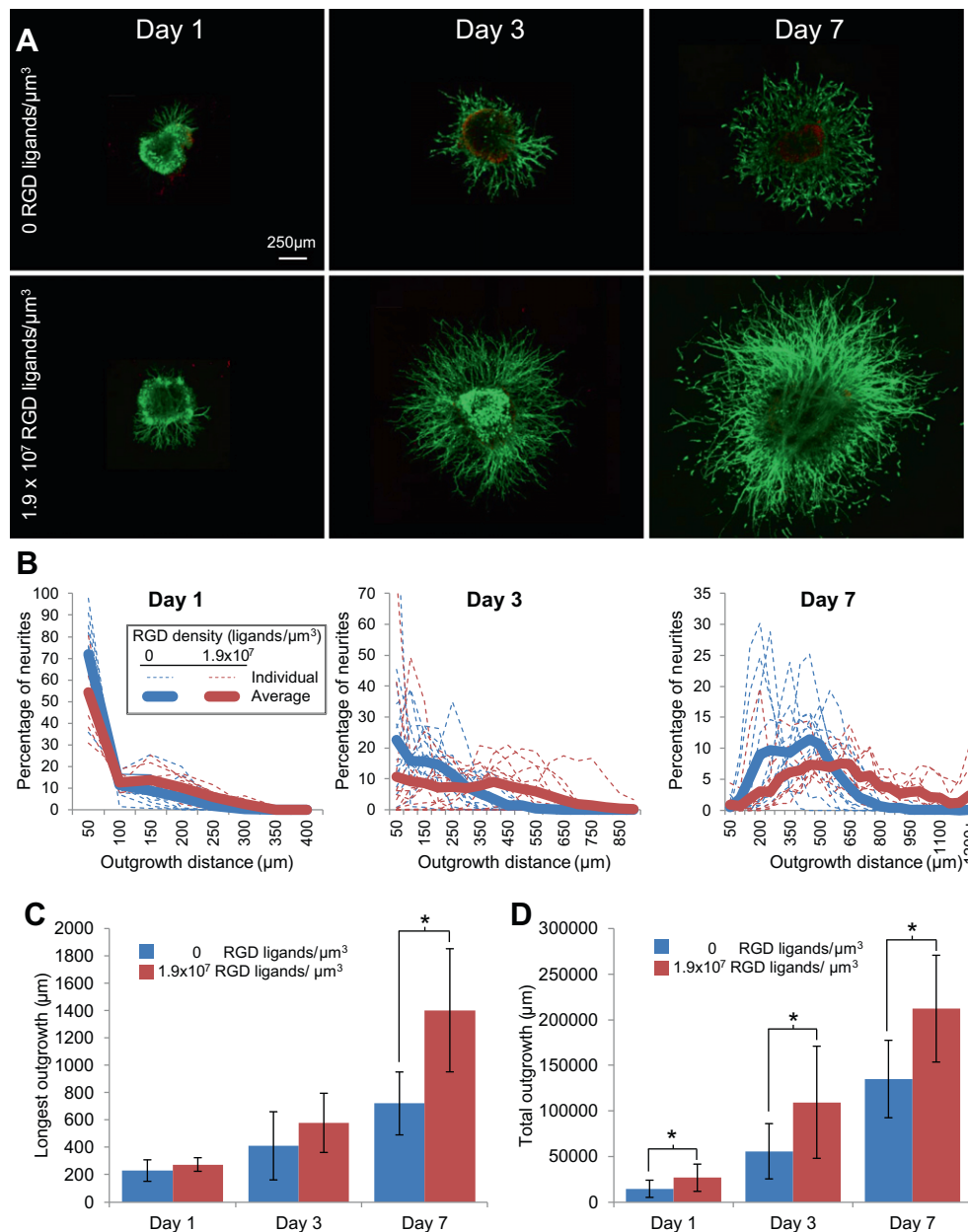
Fig. 4. Effect of cell-adhesive RGD ligand density on neurite growth in 3-D ELP hydrogels. (A) Neurites extended from the initial DRG explant in hydrogels with 0 and 1.9×10^7 cell-adhesive RGD ligands μm^{-3} over the course of 7 days culture. (B) The population distribution of neurite out-growth lengths between the two hydrogel types was statistically different at all time points as determined by Kolmogorov–Smirnov testing. Each thin, dotted line represents the percentage of neurites at each out-growth distance within a single DRG sample, whereas darker solid lines indicate the population averages. (C) The longest neurite out-growth for the two hydrogel conditions was statistically different only at 7 days. (D) When out-growth length was summed for the complete radial distribution hydrogels with 1.9×10^7 RGD ligands μm^{-3} facilitated statistically greater out-growth at all time points. Data are presented as averages ± standard deviation. $n = 8$–16 from at least four different experiments. *$P < 0.05$.
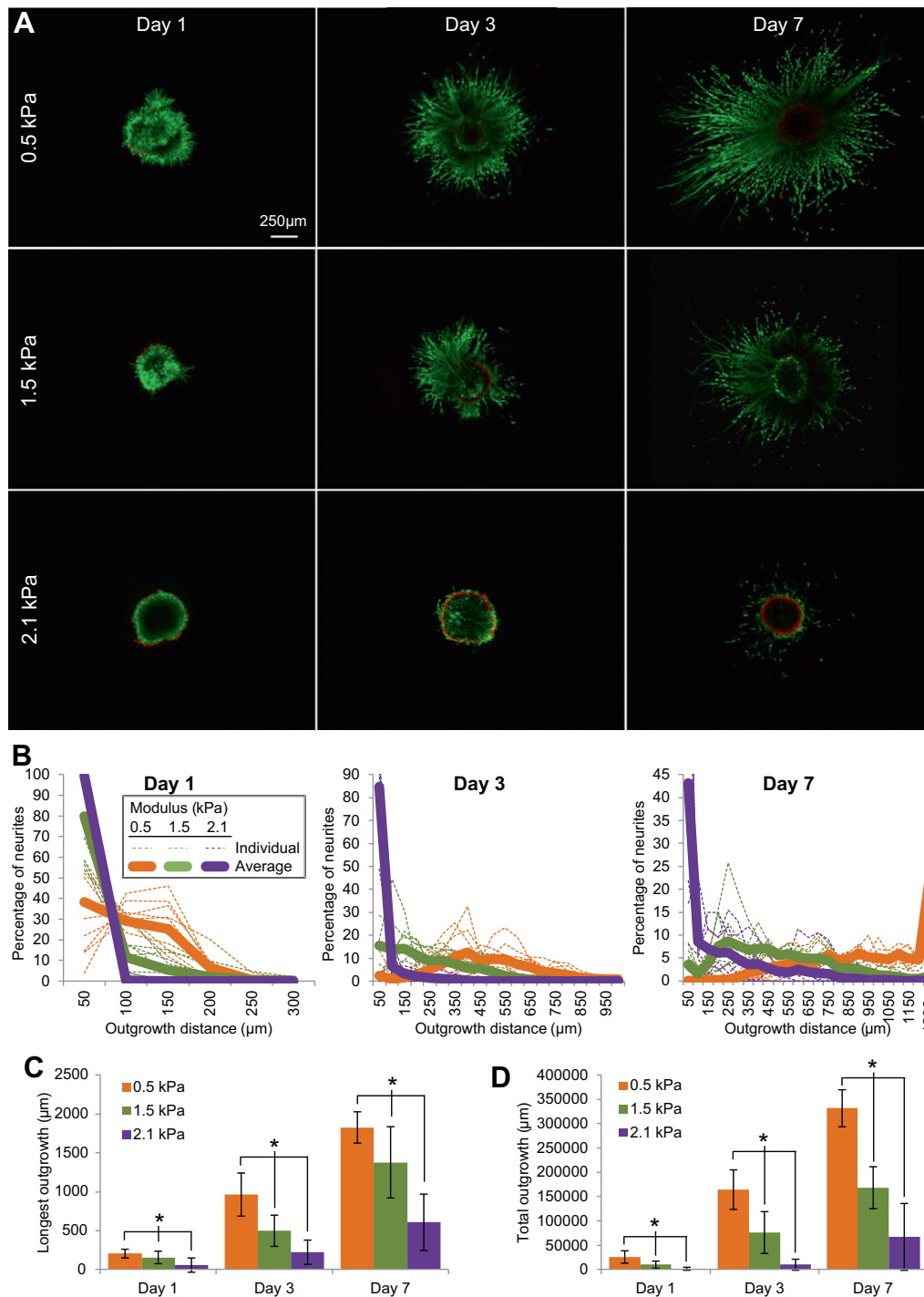
Fig. 5. Effect of matrix stiffness on neurite growth in 3-D ELP hydrogels. (A) Neurites extended by day 1 in 0.5 kPa hydrogels, by day 3 in 1.5 kPa hydrogels, and not until day 7 in 2.1 kPa hydrogels. (B) At all time points more and longer neurites were seen for decreasing hydrogel stiffness. Each hydrogel stiffness resulted in statistically different population distributions at each time point, as determined by Kolmogorov–Smirnov analysis. Each thin, dotted line represents the percentage of neurites at each out-growth distance within a single DRG sample, whereas darker solid lines indicate the population averages. (C) The longest penetration into the surrounding matrix varied significantly as a function of hydrogel stiffness. (D) Hydrogel stiffness also led to statistically different total amounts of growth at all time points. Data are presented as averages ± standard deviation. $n = 7$–12 from at least three separate experiments. *$P < 0.05$.

group, which is understood as inherent for complex biological systems, particularly those that use a heterogeneous primary tissue composed of multiple cell types. By day 3 hydrogels with RGD ligand present yielded a clear increase in length and number of neurites, with a much larger percentage of neurites found for length scales longer than 350 µm (Fig. 4B). On day 7 this effect was even more pronounced (Fig. 4B).

A limiting factor in neural regeneration is the ability to extend axons long distances over which nerves do not spontaneously regenerate. Thus we further analyzed our data to determine the longest neurite out-growth distance from each encapsulated DRG. Over the course of 7 days the 1.9×10^7 ligands µm^{-3} samples were able to promote neurite lengths of over 1400 µm (Fig. 4C). Comparing the two RGD densities, there was a statistically

significant difference in longest neurite out-growth between the two samples only on day 7 (Fig. 4C). The out-growth distance (i.e., 500–1000 μm over several days) is comparable with that previously observed in bioactive hydrogels [38,50,51].

To represent the density of neurite growth we defined the total neurite out-growth as the summation of the neurite Euclidian distances measured at each 1° interval. In contrast to the longest neurite out-growth distance, the total neurite out-growth was more than doubled at every time point when comparing the ELP materials with and without RGD ligands (Fig. 4D). This demonstrates that neurite out-growth was more uniformly distributed in the presence of the RGD ligand and also highlights the importance of characterizing multiple parameters of neurite out-growth when evaluating 3-D biomaterials. Thus, ELP hydrogels with RGD ligands promoted extension of a larger number of long neurites, which is a common goal in neural regeneration strategies.

3.5. Neurite out-growth is enhanced in more compliant ELP hydrogels

To evaluate the impact of initial hydrogel stiffness on neurite out-growth DRGs were encapsulated in ELP hydrogels of identical protein weight percent (3 wt.%) and RGD density (1.9×10^7-ligands μm^{-3}) but varied crosslink density (n = 7–12 per condition and time point from at least 3 different experiments). As observed by live/dead staining, neurite out-growth occurred by day 1 in the most compliant matrix (0.5 kPa), by day 3 in the intermediate stiffness matrix (1.5 kPa), and only rarely by day 7 in the stiffest matrix (2.1 kPa) (Fig. 5A). Kolmogorov–Smirnov analysis of the population distributions revealed statistically significant differences between all three matrices at all time points (Fig. 5B). Initial ELP hydrogel stiffness therefore has a significant effect on neurite out-growth, as decreased stiffness consistently resulted in a higher percentage of neurites at longer length scales.

To confirm our hypothesis that the majority of imaged neurons were not affected by the presence of the underlying rigid coverslip (as discussed in Section 3.2), data from day 3 samples were analyzed using two different hydrogel depths, 0–100 μm (Fig. 5) and 50–100 μm (Supplementary Fig. S1). For the Supplementary Fig. S1 analysis the 50 μm thick sections contain neurites far removed from the underlying coverslip. This depth is more than five times the length scale of a single cell ($\sim$5 × 8 μm) and is much greater than the depth previously shown to result in cellular substrate sensing (1–3.4 μm) [43,44]. Both the longest neurite out-growth and total out-growth retained statistically significant differences between the 0.5, 1.5, and 2.1 kPa hydrogels (Supplementary Fig. S1). The longest out-growth measurements are comparable with those for the full thickness analyses (Supplementary Fig. S1A and Fig. 5C), indicating that long neurite out-growth was not associated with the underlying coverslip. As expected, total out-growth measurements are about half of that for the full thickness analyses, since neurites were quantified in only half of the full observation volume (Supplementary Fig. S1B and Fig. 5D). These data confirm that the presence of the underlying glass coverslip does not statistically affect the longest neurite out-growth nor the total neurite out-growth. These data further demonstrate that the individual neuronal cells experienced a 3-D hydrogel microenvironment.

Similarly to the histograms, the longest neurite out-growth distance was significantly enhanced in the more compliant matrices across all conditions at every time point for the comprehensive, full thickness data sets (Fig. 5C). In the most compliant matrix (0.5 kPa) an average longest out-growth of 1826 μm was observed at 7 days. The decrease in stiffness also promoted a greater density of long neurites, as demonstrated by the total neurite out-growth distance (Fig. 5D). After 7 days total neurite out-growth was limited to 67,000 μm in the stiffest hydrogel, while growth was promoted to 170,000 and 332,000 μm in the 1.5 and 0.5 kPa hydrogels, respectively. Because cell viability within all ELP hydrogels was indistinguishable on day 1 (Fig. 2) and the DRG explants in the stiffest hydrogels appeared to survive well (Fig. 5A) it is unlikely that the observed differences are due to porosity limitations on diffusion of growth factors or nutrients. Although a few exceptions have been reported [52], a consistent trend has begun to emerge suggesting that more compliant biomaterials tend to promote neurite extension [24,25,31,38]. While direct comparisons with previous reports are difficult due to differences in cell type and outcome measurements, the range of mechanical stiffnesses studied here ($G' \sim$170–700 Pa, assuming a Poisson's ratio of 0.5) [53] is similar in magnitude to previous studies utilizing alginate and agarose matrices ($G' \sim$180–330 Pa) [25,32].

In this study crosslink density was used as a mechanism for varying hydrogel stiffness. In amorphous hydrogel systems, such as crosslinked ELPs, a change in crosslink density changes the mesh size, thereby affecting hydrogel stiffness as well as the diffusion rate of soluble factors through the polymer matrix. As these materials are made exclusively from recombinant proteins these hydrogels degrade via proteolysis. An increase in stiffness has been reported to alter protease secretion of encapsulated neurons [54] and may similarly alter protease activator and protease inhibitor secretion. In our system the protein weight percent, and therefore the concentration of substrate sites for proteolytic action, was kept constant across all hydrogel formulations. However, the secretion, diffusion, activation, and inactivation of cell-secreted proteases may all be altered in response to hydrogel mesh size, potentially resulting in different patterns of local matrix degradation within hydrogels of varying crosslink density. Therefore, the molecular mechanism(s) responsible for the observed differences in neurite out-growth within amorphous hydrogels of varying initial moduli cannot be identified without further studies. To this end ELP hydrogels have been designed to include different proteolytic degradation domains with tunable degradation kinetics [20]. These ELP matrices may be appropriate for future investigations into the interplay between initial hydrogel mechanics, hydrogel mesh size, local proteolytic degradation, and 3-D neurite out-growth.

3.6. Fabrication of a two-layered, composite ELP conduit

To demonstrate the potential application of these materials to fabricate nerve guides a two-layered, composite ELP conduit was constructed. ELP hydrogels can be formed within molds of any shape to create composite structures that have regions of distinct material properties [19]. Using silicone tubing and solidified agarose as our molding materials we first fabricated a hollow, cylindrical tube of 10 wt.% ELP (Fig. 6). This outer tube (length $\sim$20 mm, outer diameter $\sim$5 mm, inner diameter $\sim$3 mm) was subsequently filled with a 3 wt.% ELP solution. This two-layered composite structure was able to support its own weight and maintain the two distinct layers of ELP properties (as visualized using dyes in Fig. 6). This two-step molding technique allows fabrication of a fully ELP core–shell conduit with an outer shell (blue) that provides structure and handling ability and an inner core (red) that is suitable for 3-D neurite out-growth, as shown above. Previous work by others has demonstrated that conduit geometries can promote the alignment of neurite out-growth by physical containment [55–57], although this remains to be studied for the scaffolds shown here. It is now known that the inner lumen filler of nerve guidance conduits plays an essential role in promoting regeneration across large nerve gaps [58], highlighting the importance of a suitable biomaterial filler such as the most compliant RGD-ligand containing hydrogels we have developed here. Further ELP scaffold optimization, for example creating a topographically aligned pattern or including additional ligand sequences, may further promote
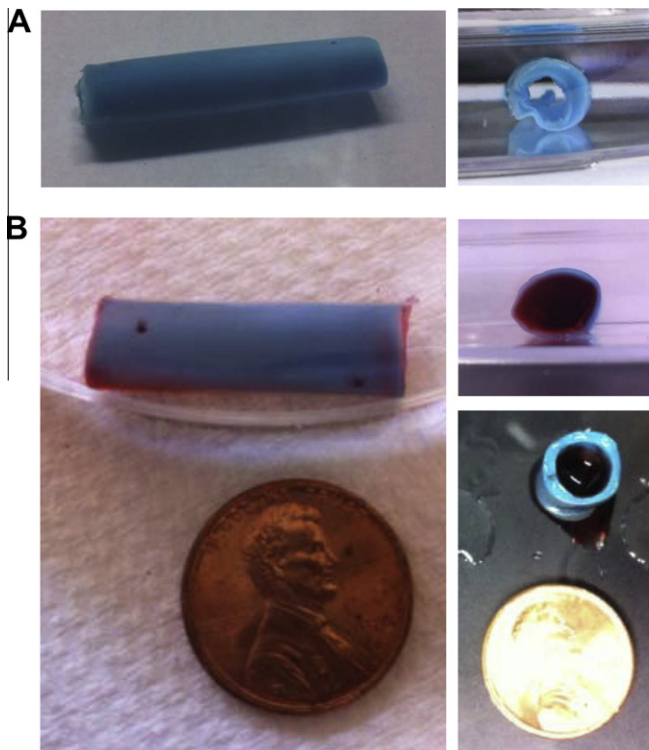
Fig. 6. Elastin-like protein hydrogels can be formed in any shape, including that of a conduit. (A) A hollow tube was molded from 10 wt.% ELP (1:1 crosslinking ratio) stained with blue food coloring to aid visualization (length ~20 mm, outer diameter ~5 mm, inner diameter ~3 mm). (B) This hollow conduit was filled with a second ELP solution (3 wt.%, 1:1 crosslinking ratio, stained red) that is suitable for neurite extension. The conduit can freely support itself (lower right), but is flexible and compliant.

neurite alignment and long axonal regeneration, both of which are thought to be critical for therapeutic biomaterials applications.

4. Conclusions

The engineered ELP hydrogels presented here combine the bioactivity and specificity of native ECM proteins with the reproducibility and predictable tailorability of synthetic polymers to create 3-D hydrogels that promote tissue growth. A family of ELP hydrogels was designed with modular bioactive and structural regions to enable the systematic synthesis and characterization of materials with specified design parameters. We here show that this ELP hydrogel enables such reductionist studies of cell–biomaterial interactions to be conducted in three dimensions. Our data demonstrate an ability to systematically and independently tailor the cell-adhesive RGD ligand density and hydrogel stiffness to tunably promote 3-D neurite out-growth. Further optimization of the RGD ligand density and elastic modulus of the ELP hydrogels may be capable of inducing even greater neurite extension.

With our chosen biological model we observed large population heterogeneity in neurite out-growth lengths. Our in-house designed analysis method clearly captured this phenomenon and enabled elucidation of statistically significant differences between various hydrogel designs. The success in inducing neurite growth to very long length scales (greater than 1 mm in compliant matrices with RGD ligands) in our 3-D ELP hydrogels is promising for the regeneration of long axonal connections. Furthermore, the density of neurite out-growth indicates that very large numbers of neurons were able to regrow axons.

This work demonstrates the versatility and responsiveness of our modularly designed ELP hydrogels for neural cell culture and supports continued development as a biomaterial tissue construct for promoting neurite growth. For example, this gelation format may be adapted to create ELP hydrogels of any shape and size allowing creation of guidance conduits supportive of aligned nerve fiber growth [55,59]. While promoting extensive neurite growth is important, only oriented growth is clinically useful. As demonstrated here, these engineered proteins can be patterned into structured devices with varying crosslinking ratios to fabricate ELP conduits filled with a neurite-permissive ELP hydrogel. Other design patterns could vary the RGD ratio or biodegradation rate [19] to create regions that promote or inhibit localized growth. Due to the matrix versatility and biospecificity ELP hydrogels may be further designed to promote the growth of other cell types of interest in neural regenerative medicine, such as oligodendrocytes, Schwann cells, and neural stem cells. Taken together, these data suggest that ELP hydrogels may be therapeutically relevant for inducing neurons to regenerate severed axons and encourages the further investigation of these biomaterials for neural regeneration applications.

Acknowledgements

Appendix A. Figures with essential colour discrimination

Certain figures in this article, particularly Figs. 1–6, are difficult to interpret in black and white. The full colour images can be found in the on-line version, at http://dx.doi.org/10.1016/j.actbio.2012.10.033.

Appendix B. Supplementary data

Supplementary data associated with this article can be found, in the online version, at http://dx.doi.org/10.1016/j.actbio.2012.10.033.

References

[1] Liu K, Tedeschi A, Park KK, He Z. Neuronal intrinsic mechanisms of axon regeneration. Annu Rev Neurosci 2011;34:131–52.
[2] Macaya D, Spector M. Injectable hydrogel materials for spinal cord regeneration: a review. Biomed Mater 2012;7:1–22.
[3] Tetzlaff W, Okon EB, Karimi-Abdolrezaee S, Hill CE, Sparling JS, Plemel JR, et al. A systematic review of cellular transplantation therapies for spinal cord injury. J Neurotrauma 2011;28:1611–82.
[4] Aurand ER, Lampe KJ, Bjugstad KB. Defining and designing polymers and hydrogels for neural tissue engineering. Neurosci Res 2012;72:199–213.
[5] Bozkurt A, Brook GA, Moellers S, Lassner F, Sellhaus B, Weis J, et al. In vitro assessment of axonal growth using dorsal root ganglia explants in a novel three-dimensional collagen matrix. Tissue Eng 2007;13:2971–9.
[6] Deister C, Aljabari S, Schmidt CE. Effects of collagen 1, fibronectin, laminin and hyaluronic acid concentration in multi-component gels on neurite extension. J Biomater Sci Polym Ed 2007;18:983–97.
[7] Willerth SM, Arendas KJ, Gottlieb DI, Sakiyama-Elbert SE. Optimization of fibrin scaffolds for differentiation of murine embryonic stem cells into neural lineage cells. Biomaterials 2006;27:5990–6003.
[8] Willits RK, Skornia SL. Effect of collagen gel stiffness on neurite extension. J Biomater Sci Polym Ed 2004;15:1521–31.
[9] Wang LZ, Gorlin J, Michaud SE, Janmey PA, Goddeau RP, Kuuse R, et al. Purification of salmon clotting factors and their use as tissue sealants. Thromb Res 2000;100:537–48.

[10] Ju YE, Janmey PA, McCormick ME, Sawyer ES, Flanagan LA. Enhanced neurite growth from mammalian neurons in three-dimensional salmon fibrin gels. Biomaterials 2007;28:2097–108.

[11] Leipzig ND, Wylie RG, Kim H, Shoichet MS. Differentiation of neural stem cells in three-dimensional growth factor-immobilized chitosan hydrogel scaffolds. Biomaterials 2011;32:57–64.

[12] Gelain F, Bottai D, Vescovi A, Zhang S. Designer self-assembling peptide nanofiber scaffolds for adult mouse neural stem cell 3-dimensional cultures. PLoS One 2006;1:e119.

[13] Silva GA, Czeisler C, Niece KL, Beniash E, Harrington DA, Kessler JA, et al. Selective differentiation of neural progenitor cells by high-epitope density nanofibers. Science 2004;303:1352–5.

[14] Mahoney MJ, Anseth KS. Three-dimensional growth and function of neural tissue in degradable polyethylene glycol hydrogels. Biomaterials 2006;27:2265–74.

[15] Foo CTSWP, Lee JS, Mulyasasmita W, Parisi-Amon A, Heilshorn SC. Two-component protein-engineered physical hydrogels for cell encapsulation. Proc Natl Acad Sci USA 2009;106:22067–72.

[16] Lampe KJ, Heilshorn SC. Building stem cell niches from the molecule up through engineered peptide materials. Neurosci Lett 2012;519:138–46.

[17] Di Zio K, Tirrell DA. Mechanical properties of artificial protein matrices engineered for control of cell and tissue behavior. Macromolecules 2003;36:1553–8.

[18] Straley KS, Heilshorn SC. Design and adsorption of modular engineered proteins to prepare customized, neuron-compatible coatings. Front Neuroeng 2009;2:1–10.

[19] Straley KS, Heilshorn SC. Dynamic, 3D-pattern formation within enzyme-responsive hydrogels. Adv Mater 2009;21:4148–52.

[20] Straley KS, Heilshorn SC. Independent tuning of multiple biomaterial properties using protein engineering. Soft Matter 2009;5:114–24.

[21] Ribeiro A, Vargo S, Powell EM, Leach JB. Substrate three-dimensionality induces elemental morphological transformation of sensory neurons on a physiologic timescale. Tissue Eng 2012;18:93–102.

[22] Lampe KJ, Mooney RG, Bjugstad KB, Mahoney MJ. Effect of macromer weight percent on neural cell growth in 2D and 3D nondegradable PEG hydrogel culture. J Biomed Mater Res A 2010;94A:1162–71.

[23] Saha K, Keung AJ, Irwin EF, Li Y, Little L, Schaffer DV, et al. Substrate modulus directs neural stem cell behavior. Biophys J 2008;95:4426–38.

[24] Gunn JW, Turner SD, Mann BK. Adhesive and mechanical properties of hydrogels influence neurite extension. J Biomed Mater Res A 2005;72A:91–7.

[25] Georges PC, Miller WJ, Meaney DF, Sawyer ES, Janmey PA. Matrices with compliance comparable to that of brain tissue select neuronal over glial growth in mixed cortical cultures. Biophys J 2006;90:3012–8.

[26] Kofron CM, Fong VJ, Hoffman-Kim D. Neurite outgrowth at the interface of 2D and 3D growth environments. J Neural Eng 2009;6:1–12.

[27] Cukierman E, Pankov R, Yamada KM. Cell interactions with three-dimensional matrices. Curr Opin Cell Biol 2002;14:633–9.

[28] Fraley SI, Feng Y, Krishnamurthy R, Kim D-H, Celedon A, Longmore GD, et al. A distinctive role for focal adhesion proteins in three-dimensional cell motility. Nat Cell Biol 2010;12:598–604.

[29] Fraley SI, Feng Y, Wirtz D, Longmore GD. Reply: reducing background fluorescence reveals adhesions in 3D matrices. Nat Cell Biol 2011;13(5):U254.

[30] Legant WR, Miller JS, Blakely BL, Cohen DM, Genin GM, Chen CS. Measurement of mechanical tractions exerted by cells in three-dimensional matrices. Nat Methods 2010;969(7):U113.

[31] Flanagan LA, Ju YE, Marg B, Osterfield M, Janmey PA. Neurite branching on deformable substrates. Neuroreport 2002;13:2411–5.

[32] Banerjee A, Arha M, Choudhary S, Ashton RS, Bhatia SR, Schaffer DV, et al. The influence of hydrogel modulus on the proliferation and differentiation of encapsulated neural stem cells. Biomaterials 2009;30:4695–9.

[33] Jung JP, Moyano JV, Collier JH. Multifactorial optimization of endothelial cell growth using modular synthetic extracellular matrices. Integr Biol 2011;3:185–96.

[34] Cunha C, Panseri S, Villa O, Silva D, Gelain F. 3D culture of adult mouse neural stem cells within functionalized self-assembling peptide scaffolds. Int J Nanomed 2011;6:943–55.

[35] Luo Y, Shoichet MS. A photolabile hydrogel for guided three-dimensional cell growth and migration. Nat Mater 2004;3:249–53.

[36] Schense JC, Hubbell JA. Three-dimensional migration of neurites is mediated by adhesion site density and affinity. J Biol Chem 2000;275:6813–8.

[37] Sakiyama SE, Schense JC, Hubbell JA. Incorporation of heparin-binding peptides into fibrin gels enhances neurite extension: an example of designer matrices in tissue engineering. FASEB J 1999;13:2214–24.

[38] Balgude AP, Yu X, Szymanski A, Bellamkonda RV. Agarose gel stiffness determines rate of DRG neurite extension in 3D cultures. Biomaterials 2001;22:1077–84.

[39] Dillon GP, Yu XJ, Sridharan A, Ranieri JP, Bellamkonda RV. The influence of physical structure and charge on neurite extension in a 3D hydrogel scaffold. J Biomater Sci Polym Ed 1998;9:1049–69.

[40] Marquardt L, Willits RK. Neurite growth in PEG gels: effect of mechanical stiffness and laminin concentration. J Biomed Mater Res A 2011;98A:1–6.

[41] Curley JL, Moore MJ. Facile micropatterning of dual hydrogel systems for 3D models of neurite outgrowth. J Biomed Mater Res A 2011;99A:532–43.

[42] Dikovsky D, Bianco-Peled H, Seliktar D. Defining the role of matrix compliance and proteolysis in three-dimensional cell spreading and remodeling. Biophys J 2008;94:2914–25.

[43] Sen S, Engler AJ, Discher DE. Matrix strains induced by cells: computing how far cells can feel. Cell Mol Bioeng 2009;2:39–48.

[44] Buxboim A, Rajagopal K, Brown AEX, Discher DE. How deeply cells feel: methods for thin gels. J Phys Condens Matter 2010;22:1–10.

[45] Betz T, Koch D, Lu YB, Franze K, Kas JA. Growth cones as soft and weak force generators. Proc Natl Acad Sci USA 2011;108:13420–5.

[46] Friedl P, Zanker KS, Brocker EB. Cell migration strategies in 3-D extracellular matrix: differences in morphology, cell matrix interactions, and integrin function. Microsc Res Tech 1998;43:369–78.

[47] Webber C, Zochodne D. The nerve regenerative microenvironment: early behavior and partnership of axons and Schwann cells. Exp Neurol 2010;223:51–9.

[48] McKeon RJ, Schreiber RC, Rudge JS, Silver J. Reduction of neurite outgrowth in a model of glial scarring following CNS injury is correlated with the expression of inhibitory molecules on reactive astrocytes. J Neurosci 1991;11:3398–411.

[49] Meijering E. Neuron tracing in perspective. Cytometry A 2010;77A:693–704.

[50] Sarig-Nadir O, Seliktar D. Compositional alterations of fibrin-based materials for regulating in vitro neural outgrowth. Tissue Eng A 2008;14:401–11.

[51] Sang-Nadir O, Seliktar D. The role of matrix metalloproteinases in regulating neuronal and nonneuronal cell invasion into PEGylated fibrinogen hydrogels. Biomaterials 2010;31:6411–6.

[52] Leach JB, Brown XQ, Jacot JG, DiMilla PA, Wong JY. Neurite outgrowth and branching of PC12 cells on very soft substrates sharply decreases below a threshold of substrate rigidity. J Neural Eng 2007;4:26–34.

[53] Urry DW, Hugel T, Seitz M, Gaub HE, Sheiba L, Dea J, et al. Elastin: a representative ideal protein elastomer. Philos Trans R Soc Lond Ser B Biol Sci 2002;357:169–84.

[54] Man AJ, Davis HE, Itoh A, Leach JK, Bannerman P. Neurite outgrowth in fibrin gels is regulated by substrate stiffness. Tissue Eng A 2011;17:2931–42.

[55] Bellamkonda RV. Peripheral nerve regeneration: an opinion on channels, scaffolds and anisotropy. Biomaterials 2006;27:3515–8.

[56] Gelain F, Panseri S, Antonini S, Cunha C, Donega M, Lowery J, et al. Transplantation of nanostructured composite scaffolds results in the regeneration of chronically injured spinal cords. ACS Nano 2011;5:227–36.

[57] Wood MD, MacEwan MR, French AR, Moore AM, Hunter DA, Mackinnon SE, et al. Fibrin matrices with affinity-based delivery systems and neurotrophic factors promote functional nerve regeneration. Biotechnol Bioeng 2010;223:970–9.

[58] Jiang X, Lim SH, Mao HQ, Chew SY. Current applications and future perspectives of artificial nerve conduits. Exp Neurol 2010;223:86–101.

[59] Deumens R, Bozkurt A, Meek MF, Marcus MAE, Joosten EAJ, Weis J, et al. Repairing injured peripheral nerves: bridging the gap. Prog Neurobiol 2010;92:245–76.